

Use of direct numerical simulation (DNS) data to investigate spatial resolution issues in measurements of wall-bounded turbulence

C C Chin, N Hutchins, A S H Ooi and I Marusic

Department of Mechanical and Manufacturing Engineering, University of Melbourne, Victoria 3010, Australia

E-mail: nhu@unimelb.edu.au

Received 1 May 2009, in final form 1 September 2009

Published 25 September 2009

Online at stacks.iop.org/MST/20/115401

Abstract

The effect of limited spatial resolution for hot-wire anemometry (HWA) is investigated by analysing the two-dimensional energy spectra from direct numerical simulation (DNS) of turbulent channel flow at $Re_\tau \approx 950$. Various spanwise filter lengths are applied to the streamwise velocity components in order to mimic the limited spatial resolution of a single-normal hot-wire experiment. Clear attenuation of the small-scale DNS energy is observed as the filter length is increased and good agreement is noted between the missing energy from filtered DNS and that from hot-wire experiments over a range of sensing lengths. The missing energy in the near-wall region is shown to be highly anisotropic in nature, thus bringing into question existing correction schemes that rely on small-scale isotropic flow assumptions. An empirical model of the missing streamwise component energy spectra is formulated, as a function of wire length, and is shown to be useful as a new correction function for the missing energy and streamwise turbulence intensity at the near-wall energetic peak.

Keywords: hot-wire anemometry, spatial resolution, energy spectra, wall-bounded turbulence

(Some figures in this article are in colour only in the electronic version)

1. Introduction

The accurate measurement of first- and second-order statistics in a turbulent boundary layer is important in order to further advance the fundamental knowledge in this area. Investigations of flow control, heat transfer and attempts to produce more accurate theoretical models all rely on an ability to accurately measure statistics in the near-wall region of these flows. Though novel optical techniques (such as laser Doppler velocimetry [1] and particle image velocimetry [2]) are now commonly employed to measure statistics in turbulent flows, hot-wire anemometry (HWA) still remains the most popular experimental technique for turbulent boundary layer research given its unsurpassed temporal and spatial resolution. Even though HWA technology and methodology has continued

to improve, there have been discrepancies in measurements reported in the literature by different groups of researchers. Insufficient spatial resolution is known to affect the accuracy of hot-wire measurements and could account for some of the discrepancies in published results. The earliest report on effects of spatial resolution is by Dryden *et al* [3]. Later, this work was extended by Frenkiel [4], Wyngaard [5], Johansson and Alfredsson [6], Ligrani and Bradshaw [7], Citriniti and George [8], Chew *et al* [9] and most recently Hutchins *et al* [10].

Of these, perhaps the most well-known and well-cited study is that by Ligrani and Bradshaw [7] (henceforth referred to as LB87) which details an extensive study of the effects of wire length, l , on the data obtained from single-normal hot-wire experiments. The measurements of LB87 were

carried out at Reynolds number based on momentum thickness, $Re_\theta = 2620$ and at limited distances from the wall. Since the measurements were conducted using single-normal hot-wires, the conclusions were limited to the streamwise component of velocity. It was reported that with a viscous-scaled wire length (l^+) less than 20 the error in the measured root-mean-squared turbulence intensity is less than 4% (the superscript '+' denotes scaling with the viscous length scale, ν/U_τ , where ν is viscosity and U_τ is friction velocity). LB87 also suggested that the length-to-diameter (l/d) should be greater than 200 to isolate the effect of conduction; similar findings have been reported by Chew *et al* [9].

The attenuation in turbulence intensity as a result of the effect of wire length has led workers to formulate corrections for the turbulence measurements based on streamwise information and the assumption of local isotropy [5]. In formulating models to estimate spatial resolution errors for various probe configurations, Ewing and George [11] observed that assumptions of isotropy could greatly affect the predicted result. In order to obtain a more complete picture of the effects of spatial resolution for a single-normal hot-wire sensor, it is imperative to consider the width of the energetic fluctuations, as compared to the spanwise integral length of the sensor element. Since isotropic flow assumptions are not applicable in turbulent boundary layers, this requires spectral information in the spanwise direction (i.e. we need information about the energy contribution at each spanwise wavenumber, k_y^1). In general, such information is not readily available from experiments. On the other hand, spanwise information can be readily obtained from DNS data. Studies such as those conducted by Abe *et al* [12] and del Álamo *et al* [13] have shown that the spanwise spectral information of the streamwise velocity fluctuation is a complex function of distance from the wall and Reynolds number.

Previous studies have been conducted using DNS data to evaluate hot-wire performance in wall-bounded turbulence. This includes the study of Suzuki and Kasagi [14] who used DNS from a turbulent channel flow at low Reynolds number to quantify errors in near-wall hot-wire measurements, and Moin and Spalart [15] who used DNS data from a turbulent boundary layer to estimate the accuracy of cross-wire probes. More recently, Burattini *et al* [16] used DNS data to investigate the effect of spatial resolution on the hot-wire measured velocity derivative skewness in homogeneous isotropic turbulence. Also Vukoslavčević *et al* [17] employed a DNS database to simulate spatial resolution effects (on both velocity and velocity gradient measurements) made with a multi-wire sensor. Other studies using DNS for hot-wire corrections are reviewed by Moin and Mahesh [18].

In this paper, the effect of hot-wire spatial resolution in wall-bounded turbulence will be investigated using recent channel flow data from the DNS study of del Álamo *et al* [13] at a moderately high Reynolds number ($Re_\tau = 934$). The DNS data are spatially averaged (filtered) in the spanwise direction in order to simulate the averaging encountered by

different single-normal hot-wire lengths. The experimental data reported in LB87 are compared against the filtered DNS data, which are nominally at the same Reynolds number. One should note that the experiment carried out by LB87 is in a zero pressure gradient turbulent boundary layer whilst the DNS data are from a turbulent channel flow. It is commonly assumed that at sufficient Reynolds numbers, the near-wall region will be similar in channels and boundary layers. However, recent studies have revealed differences in the large-scale structure between internal and external geometries [19, 20]. These differences are most prominent in the outer flow but also seem to extend into the near-wall region. It is important to remain aware of these differences between internal and external geometries when considering the comparison between the filtered DNS and the experimental results of LB87.

This study is limited to wall-normal locations of $z^+ \approx 15$ and 120. It is widely accepted that the peak turbulence kinetic energy occurs at a wall-normal location of $z^+ \approx 15$. This peak in energy is mainly due to the near-wall cycle of streaks and quasi-streamwise vortices as documented by Kline *et al* [21] and Jiménez and Pinelli [22]. The wall-normal location $z^+ = 120$ is selected since, at this Reynolds number, it represents the approximate mid-point of the logarithmic region.

Hutchins *et al* [10] showed the effects of attenuation on the turbulence intensity profile ($\overline{u^2}/U_\tau^2$) due to insufficient spatial resolution, demonstrating that the turbulence intensity is a function of both the hot-wire length and the Reynolds number. In the same paper, they investigated the one-dimensional streamwise energy spectra for different wire lengths and highlight the missing spectral energy due to attenuation.

In this study, we characterize the lost spectral energy due to insufficient spatial resolution in a two-dimensional wavenumber space and provide an empirical correction factor to account for the lost turbulent intensity as a function of wire length.

2. Methodology

The DNS data used in this study have a friction Reynolds number, $Re_\tau = U_\tau \delta / \nu = 934$, where δ is the channel half-height. The size of the computation box is $L_x \times L_y \times L_z = 8\pi\delta \times 3\pi\delta \times 2\delta$ with grid points $N_x \times N_y \times N_z = 3072 \times 2304 \times 385$ in the x , y and z directions. The streamwise and spanwise grid spacings are $\Delta x^+ \approx 7.6$ and $\Delta y^+ \approx 3.8$, respectively. In the wall-normal direction, the grid spacing increases from $\Delta z^+ \approx 0.03$ at the wall to a maximum $\Delta z^+ \approx 7.6$ at the centre of the channel (with N_z Chebyshev polynomials). Further details of the DNS and the numerical method can be found in del Álamo *et al* [13].

The attenuation due to different wire lengths is simulated by spatially averaging the DNS data in the spanwise direction according to the desired pseudo wire length (in viscous length). The spanwise grid spacing of the DNS data is $d_y^+ \approx 3.8$; hence, the filter lengths are limited to integer multiples of d_y^+ . The filter lengths considered for the DNS data range from $l^+ \approx 11.5$ ($3d_y^+$), 19.1 ($5d_y^+$), 34.3 ($9d_y^+$) and 57.3 ($15d_y^+$). The filtering process is performed by spanwise averaging the instantaneous

¹ Here we define the streamwise, spanwise and wall-normal directions as x , y and z , respectively with the corresponding fluctuating velocity components u , v and w .

streamwise velocity (U) across the desired filter length. The broadband intensity and energy spectra are then calculated from the resulting filtered velocity fields. The streamwise turbulence intensity (denoted by $\overline{u^2}^+$) has been calculated from the filtered DNS data at all 192 wall-normal locations. Energy spectra are calculated at $z^+ = 15$ and $z^+ = 120$. The one-dimensional streamwise premultiplied energy spectra is given by

$$\phi_{uu}(k_x, z) = k_x \langle \hat{u}(k_x, z) \hat{u}^*(k_x, z) \rangle. \quad (1)$$

The premultiplied two-dimensional energy spectra can be calculated using

$$\Phi_{uu}(k_x, k_y, z) = k_x k_y \langle \hat{u}(k_x, k_y, z) \hat{u}^*(k_x, k_y, z) \rangle, \quad (2)$$

where k_x and k_y are the streamwise and spanwise wavenumbers, $\langle \rangle$ denotes spatial and temporal average, \hat{u} denotes the Fourier transform of u (which can be the filtered or unfiltered velocity field) and $*$ denotes the complex conjugate.

Compared to experimental methods, two-dimensional energy spectra can be readily obtained from DNS, which provide volumetric data of all three velocity components. However, the convergence of the two-dimensional energy spectra are difficult to achieve, especially at greater wall-normal distances where large-scale structures are dominant, and yet occurrences of these largest scales are limited within the available DNS volumes. In order to ensure better convergence of the two-dimensional statistics, we have employed an ‘overlapping’ method within the data plane of interest ($z^+ \approx 15$ and 120) and a composite construction of the final spectra using variable window sizes. A window (size $x_{\text{win}} \times y_{\text{win}}$) is selected on the xy plane and the two-dimensional spectra calculation is performed within that window. This window is then shifted in the streamwise direction, by a preset Δx which overlaps the previous window location (by $x_{\text{win}} - \Delta x$), and the process is reiterated. The same procedure is applied in the spanwise direction with a preset Δy (spanwise overlap $y_{\text{win}} - \Delta y$). This process is reiterated until the entire data plane is processed. The mean energy spectra for that individual window size is then computed. For a given window size, this shifting and overlapping procedure provides more realizations from the available set of data, leading to improved convergence of the ensemble averaged spectra. This process is repeated for different window sizes, starting from the smallest up to $4\pi\delta \times 1.5\pi\delta$. The spectra for each window size are then compiled into a single composite plot that covers the entire available wavelength space, up to $\lambda_x = 4\pi\delta$ and $\lambda_y = 1.5\pi\delta$ ($\lambda = 2\pi/k$). The rationale for this composite technique is to ensure that the large-scale energy spectra is captured (requiring large x_{win} and y_{win}) without compromising the convergence of the small-scale energy (which converge better with small x_{win} and y_{win}).

3. Effect of the wire length on turbulence intensity

The comparison of the turbulence intensity, $\overline{u^2}^+$, for DNS data (solid symbol) and LB87 (open symbol) is shown in figure 1. Note that the results from DNS correspond to wall-normal distance $z^+ \approx 15$ whereas data from LB87 are at $z^+ \approx 17$.

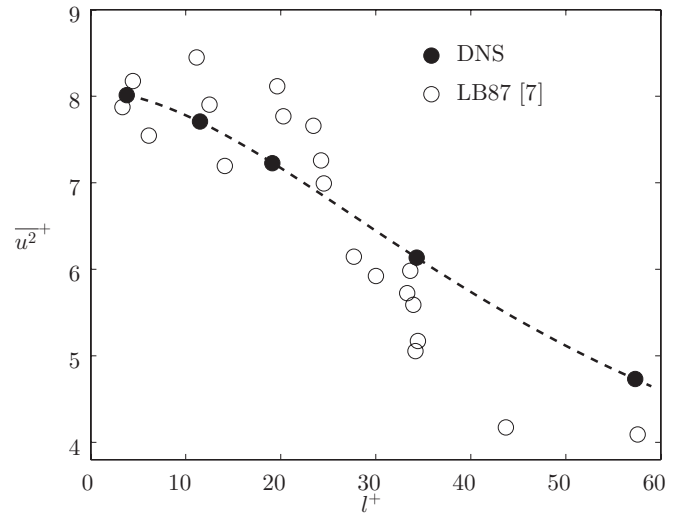


Figure 1. Spatial averaging effect on $\overline{u^2}^+$ for different filter sizes, l^+ , at a wall-normal distance of $z^+ \approx 15$ (DNS) and $z^+ \approx 17$ (LB87). The dashed line is the best fit through the DNS data set corresponding to equation (3).

Only those data from LB87 where l/d is greater than 200 are shown in figure 1 (to isolate the effect of l/d). It should also be noted that the use of a spanwise boxcar filter to spatially average the DNS data is an imperfect approximation of the spatial averaging due to a real hot wire. The temperature profile across a hot wire will produce an effective length that is shorter than the actual length of the sensor [23]. For a given l^+ we would expect the boxcar filter to be slightly more aggressive than the filtering due to a hot wire of comparable length. The attenuation of the turbulence intensity increases with increasing l^+ as one would expect. For the data of LB87, it can be seen that as l^+ exceeds 25, and the effect of spatial resolution causes an abrupt increase in attenuation on the turbulence intensity, $\overline{u^2}^+$. The DNS data show a similar trend of decreasing turbulence intensity as the filter size increases. Ligrani and Bradshaw report that for $l^+ < 20$ – 25 , the error in the mean-squared streamwise broadband intensity is less than 8%. The DNS data seem to indicate that for $l^+ \approx 19$, the error is 10%. The suggestion from the DNS data is that the error due to viscous-scaled wire lengths $O(20)$ is slightly larger than that suggested in the conclusions of LB87. Similar findings were reported in Hutchins *et al* [10] where the error expected for $l^+ = 20$ is approximately 10%. Here we describe the missing streamwise turbulent energy at $z^+ = 15$ caused by a wire of length l^+ using a third-order polynomial of the form

$$\overline{u_{\text{missing}}^2}^+ = Al^{+3} + Bl^{+2} + Cl^+ + D, \quad (3)$$

which by least-squares regression fit returns the constants $A = -1.94 \times 10^{-5}$, $B = 1.83 \times 10^{-3}$, $C = 1.76 \times 10^{-2}$ and $D = -9.68 \times 10^{-2}$. The dashed line in figure 1 shows the viscous-scaled turbulent energy measured with a given wire size, defined as

$$\overline{u_{l^+}^2}^+ = \overline{u_{\text{actual}}^2}^+ - \overline{u_{\text{missing}}^2}^+, \quad (4)$$

where $\overline{u_{\text{actual}}^2}^+$ is the energy one would expect to measure in the absence of spatial filtering (the unattenuated result). We

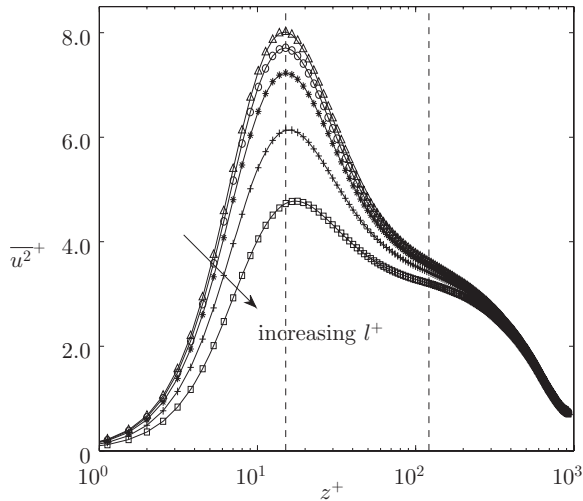


Figure 2. Comparison of streamwise turbulence intensity profiles for different filter lengths, $l^+ \approx 3.8$ (Δ), 11.5 (\circ), 19.1 (\star), 34.3 ($+$) and 57.3 (\square); arrow indicates increasing filter length (l^+), and the dashed lines are at $z^+ \approx 15$ and 120 ($z/\delta \approx 0.12$).

here assume that the original DNS data, with a spanwise grid spacing of 3.8 wall units, are unfiltered. Using this expression, the missing turbulence intensity can be estimated in experimental results given the wire length. Strictly speaking, it is noted that this expression is true only at the given Reynolds number. Hutchins *et al* [10] suggest that at $z^+ = 15$, the measured turbulent energy $\overline{u_{l^+}^2}$ is a function of l^+ , Re_τ and l/δ . However, it is noted that only $\overline{u_{actual}^2}$ is a function of Re_τ , and they find that, provided l/δ is small, the missing energy $\overline{u_{missing}^2}$ can be approximated by a function of l^+ . This would seem to suggest that equation (3) might be applicable to higher Reynolds numbers provided l/δ is small (later results in section 6 imply that this function can give reasonable predictions over extended Reynolds number ranges, at least up to $Re_\tau \approx 7000$). To use equation (3) to correct an attenuated turbulent energy $\overline{u_{l^+}^2}$ measured at $z^+ \approx 15$, one would simply calculate $\overline{u_{missing}^2}$ using equation (3) and then add this back to the raw measured intensity ($\overline{u_{l^+}^2}$) to yield the estimated true value of turbulent intensity $\overline{u_{actual}^2}$.

In figure 2, the turbulence intensity profiles from the filtered DNS are shown as a function of increasing filter length l^+ . The direction of the arrow indicates increasing filter length. The dashed lines are at wall-normal locations of $z^+ \approx 15$ and 120. The peak streamwise turbulence intensity $\overline{u^2}$ is seen to be greatly attenuated in the near-wall region at $z^+ \approx 15$ (as shown in figure 1); however, the corresponding attenuation at $z^+ \approx 120$ is significantly less. For example a filter length of $l^+ \approx 57.3$ produces 41% attenuation at $z^+ \approx 15$, compared to just 11% at $z^+ \approx 120$. The percentage attenuations at $z^+ = 15$ and 120 are tabulated in table 1. These findings emphasize that limited spatial resolution has the greatest effect on the measured turbulent energy in the near-wall region. This is as expected since finite wire size will have the greatest effect on the small scales, which are predominantly located in the near-wall region.

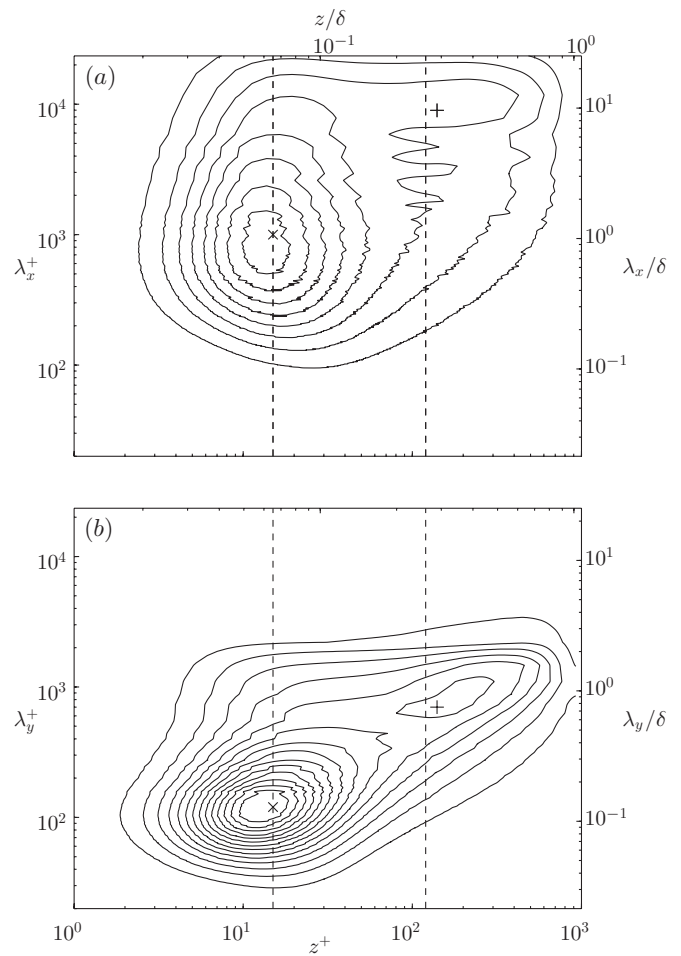


Figure 3. Premultiplied one-dimensional energy spectra as a function of the wall-normal location and (a) streamwise wavelength λ_x ; (b) spanwise wavelength λ_y . The contour maps are from $\phi_{uu}/U_\tau^2 = 0.3$ with an increment of 0.25. The dashed lines are at the wall-normal location as in figure 2.

Table 1. Tabulated error as a percentage (%) for different wire lengths for $z^+ \approx 15$ and 120.

Filter length (l^+)	Symbol	$\overline{u^2}^+$	
		($z^+ \approx 15$)	($z^+ \approx 120$)
3.8 (unfiltered)	Δ	–	–
11.5	\circ	3.8	0.7
19.1	\star	9.8	2.0
34.3	$+$	23.5	5.4
57.3	\square	41.0	11.3

4. Premultiplied one-dimensional energy spectra

The premultiplied one-dimensional energy spectra of streamwise velocity fluctuations are shown in figures 3(a) and (b) as functions of streamwise and spanwise wavelength (λ_x^+ and λ_y^+), respectively, and also the distance from the wall. The premultiplied spectra are scaled with U_τ^2 . The contour levels on these energy maps show the magnitude of the premultiplied spectra at each wavelength (y-axis) and each wall-normal location (x-axis). Two distinctive energy peaks are observed. Hutchins and Marusic [24] have referred to these two peaks

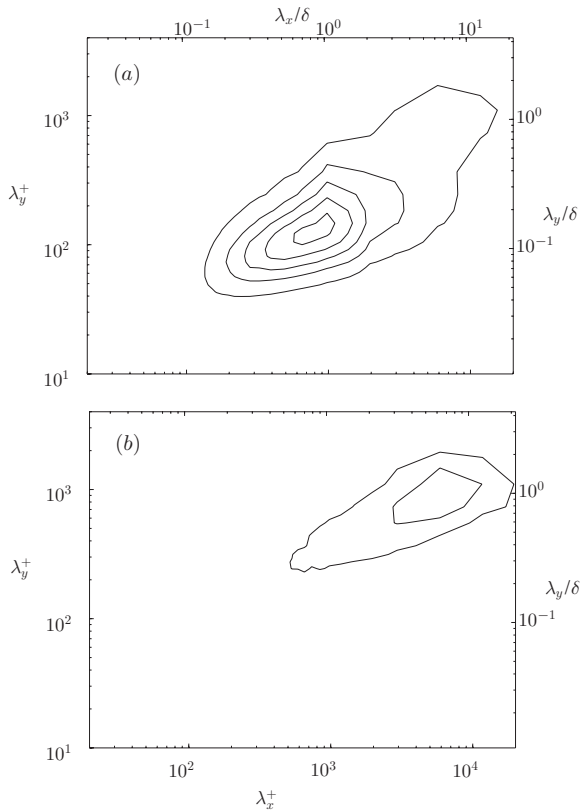


Figure 4. Premultiplied two-dimensional energy spectra (unfiltered, $l^+ \approx 3.8$) at (a) wall-normal location of $z^+ \approx 15$ and (b) wall-normal location of $z^+ \approx 120$. The contour maps for both are from $\Phi_{uu}^+ = 0.2$ with an increment of 0.2.

as the ‘inner site’, referring to the near-wall energy peak, and the ‘outer site’, which is defined as the outer energy peak away from the wall. In terms of streamwise wavelength (λ_x), Hutchins and Marusic [24] report that the ‘inner site’ is fixed in viscous coordinates at $z^+ \approx 15$ and $\lambda_x^+ \approx 1000$, in agreement with the present results shown in figure 3(a). The spectra as a function of the spanwise wavelength shown in figure 3(b) indicate that this ‘inner site’ (marked with the symbol ‘×’) is also fixed at $\lambda_y^+ \approx 120$, close to the reported value for low-speed streak spacing of 100 viscous units (e.g. Kline *et al* [21]).

For the DNS channel data, figure 3 indicates that a broad ‘outer site’ occupies the outer-scaled coordinate range $z \approx 0.15\text{--}0.2\delta$, $\lambda_x \approx 10\delta$ and $\lambda_y \approx 0.75\text{--}1.2\delta$. For zero pressure-gradient flat-plate turbulent boundary layers at higher Reynolds numbers ($Re_\tau \approx 7300$), Hutchins and Marusic [24] report that the ‘outer site’ is located at $z \approx 0.06\delta$ and $\lambda_x^+ \approx 6\delta$. The differences observed here are explained by Monty *et al* [19, 20] who show that the large-scale structures attain a greater length (and at a greater distance from the wall) in channel flow than that for turbulent boundary layers.

5. Premultiplied two-dimensional energy spectra at $z^+ \approx 15$

Figure 4(a) and (b) show the unfiltered ($l^+ \approx 3.8$) two-dimensional premultiplied u energy spectra at wall-normal

location $z^+ \approx 15$ and 120, respectively. The superscript ‘+’ in figure 4 denotes scaling of the two-dimensional premultiplied spectra by friction velocity ($\Phi_{uu}^+ = \Phi_{uu}/U_\tau^2$). All contour lines begin at $\Phi_{uu}^+ = 0.2$ and increase in steps of 0.2. Comparing the two plots in figure 4, it is clear that the peak energy occurs at larger λ_x^+ and λ_y^+ at $z^+ \approx 120$, as compared to $z^+ \approx 15$, indicating that larger scale structures dominate within the logarithmic region. This behaviour is as predicted from figure 3.

Figure 5 shows the premultiplied two-dimensional energy spectra Φ_{uu}^+ at $z^+ = 15$, for different filter lengths of $l^+ \approx 11.5$, 34.3 and 57.3. Column (a) represents the filtered energy spectra and column (b) represents the missing energy spectra. Note that the contour levels are different for each column. The contour scaling for column (a) is as given in figure 4 whereas for (b), the contour levels begin at 0.02 with increments of 0.1 (these smaller increments are used to highlight the missing energy). As the filter length is increased, figure 5(a) clearly illustrates the attenuation of small-scale energy in the premultiplied two-dimensional energy spectra. The ‘inner site’ location in the two-dimensional spectra (which for unfiltered data is located at $\lambda_x^+ \approx 1000$ and $\lambda_y^+ \approx 120$) is shifted to larger wavelengths as the filter length (l^+) is increased. An arbitrary point ($\lambda_x^+ \approx 1200$, $\lambda_y^+ \approx 200$) denoted by the ‘×’ symbol is chosen to illustrate this effect. As filter length increases from top to bottom, we see the peak shifting towards the ‘×’ symbol. Thus, it is clear that in experiments, a larger wire length will cause a pseudo peak in the spectra that is at larger wavelengths than the true unfiltered ‘inner’ energetic peak.

We can obtain a clearer understanding of the effects of insufficient spatial resolution on the premultiplied two-dimensional energy spectra by studying the missing energy shown in figure 5(b) (indicating the difference between figure 4(a) and figure 5(a)). In general, the missing energy is seen to be centred around streamwise length scales (λ_x^+) that are approximately eight times longer than the corresponding spanwise length scales (λ_y^+). Thus the primary effect of increasing wire size seems to be an attenuation of the elongated streaks due to the near-wall cycle. This highlights the highly anisotropic nature of the flow and clearly brings into question correction schemes relying on isotropic assumptions, such as that proposed by Wyngaard [5]. The attenuation seems to be centred around the ‘inner site’ and for the filter sizes shown, there is very little sign of attenuation around the outer site at $\lambda_y \approx 0.75\delta$. The ‘+’ symbol, at an arbitrary location ($\lambda_y^+ \approx 500$, $\lambda_x^+ \approx 100$), is plotted in figure 5(b) to demonstrate that the peak-missing 2D energy shifts in a manner similar to that shown for the peak-filtered 2D energy (a).

6. Model for missing energy

Most previous corrections for spatial resolution effects have been based solely on streamwise information (as discussed earlier). Here the DNS data afford us spanwise information as well, which is critical to fully understand the spanwise averaging effect of a single-normal hot wire of finite size.

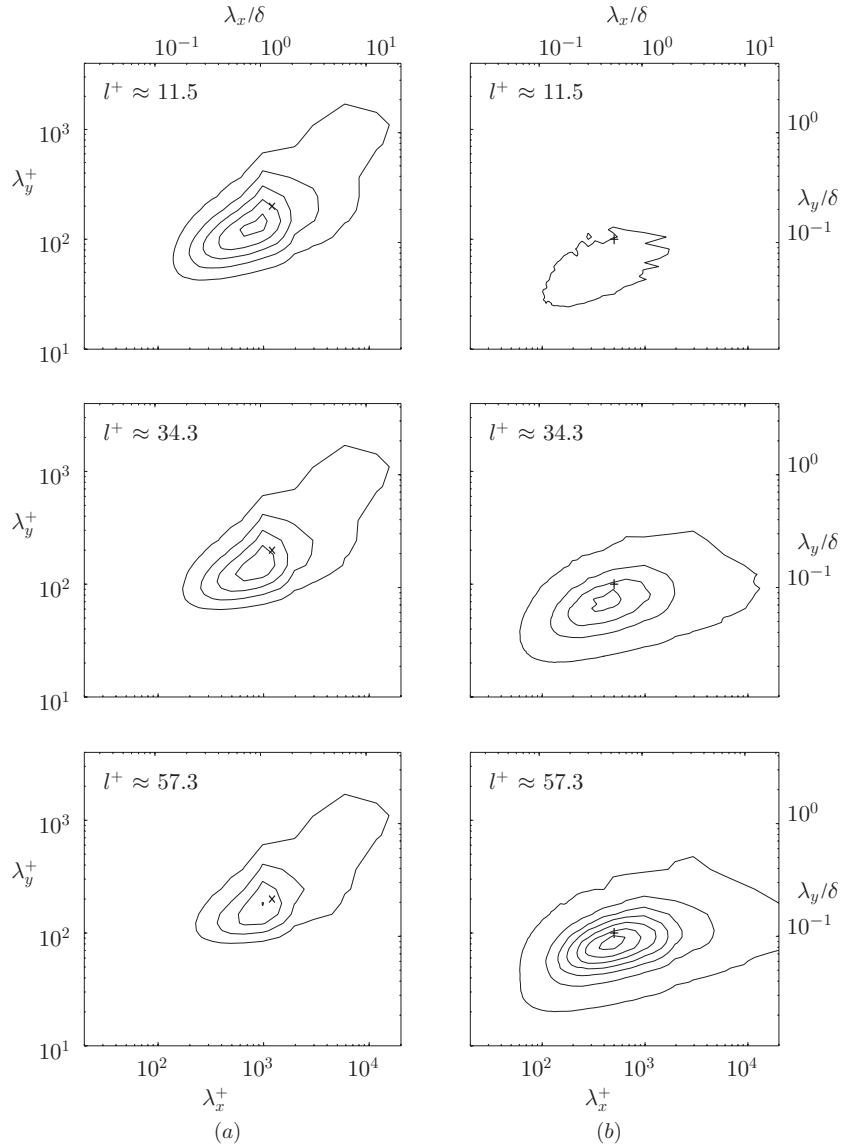


Figure 5. Premultiplied two-dimensional energy spectra of streamwise fluctuating velocity, Φ_{uu}^+ ; (a) filtered energy spectra, contour maps are as given in figure 4, and (b) missing energy spectra, contour maps are from $\Phi_{uu}^+ = 0.02$ with an increment of 0.1, for different filter lengths (l^+) at wall-normal location $z^+ \approx 15$.

The 2D information also enables us to separate the near-wall small-scale events from the larger scale superimposed energy, even at the relatively low Reynolds numbers (low-scale separation) of the DNS data. As an example, figure 5 clearly shows that a wire of length $l^+ = 57.3$ causes some attenuation of streamwise wavelengths at $\lambda_x \approx 10\delta$. In the absence of spanwise information, we may have incorrectly concluded that this implies some attenuation of the ‘outer site’, (which in figure 3 is noted to occur at $\lambda_x \approx 10\delta$). However, the 2D spectra maps show that this attenuation at long λ_x is centred at spanwise wavelengths associated with the near-wall scales ($\lambda_y^+ \approx 120$), and there is no attenuation at the ‘outer site’.

From figure 5(b), it is observed that the missing 2D premultiplied energy spectra resemble a shape close to a symmetrical Gaussian along the λ_y^+ axis, and a skewed

Gaussian along the λ_x^+ axis, with a slight rotation counter-clockwise in the log–log space. Therefore, it seems promising to model the missing Φ_{uu}^+ energy using an empirical expression of the form

$$f(\lambda_x^+, \lambda_y^+, l^+) = A \exp\left(-\left[\frac{(\alpha - \alpha_0)^2}{\sigma_\alpha} + \frac{(\beta - \beta_0)^2}{\sigma_\beta}\right]\right). \quad (5)$$

From curve-fitting to the filtered DNS data, we obtain the following expressions for the constants:

$$A = -4.9 \times 10^{-6}(l^{+3}) + 5.5 \times 10^{-4}(l^{+2}) - 0.001(l^+) + 0.0272$$

$$\alpha = 0.9553 \log_{10}(\lambda_x^+) + 0.2955 \log_{10}(\lambda_y^+) - 0.45$$

$$\beta = -0.2955 \log_{10}(\lambda_x^+) + 0.9553 \log_{10}(\lambda_y^+) + 0.86$$

$$\alpha_0 = \log_{10}(3.6l^+ + 280)$$

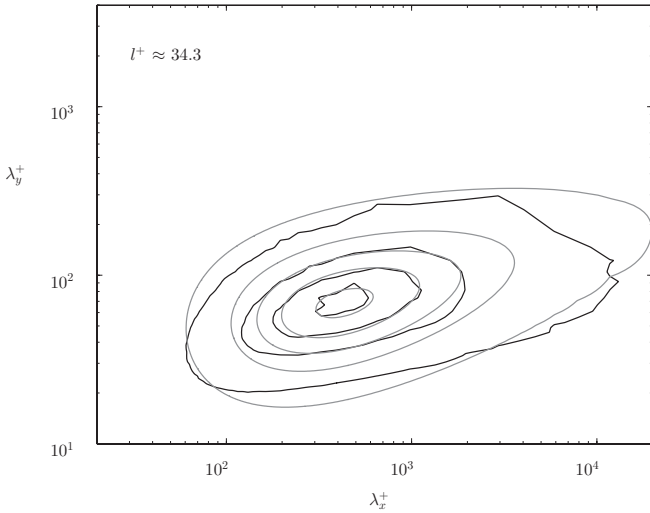


Figure 6. Comparison of missing premultiplied energy Φ_{uu}^+ at $z^+ = 15$ and for $l^+ \approx 34.3$ as modelled by the empirical equation (5) (grey line) against DNS data (black line) at the wall-normal distance $z^+ \approx 15$.

$$\beta_0 = \log_{10}(0.3l^+ + 58)$$

$$\sigma_\alpha = \log_{10}(\lambda_x^+)^{1/C} / D$$

$$\sigma_\beta = 0.1$$

$$C = 3.7 \times 10^{-6}(l^+)^3 - 1.5 \times 10^{-4}(l^+)^2 + 3.3 \times 10^{-3}(l^+) + 0.57$$

$$D = 1.3 \times 10^{-3}(l^+)^2 - 0.2712(l^+) + 17.637.$$

It is noted that these expressions are not a function of the wall-normal distance (z^+) and are applicable only at $z^+ \approx 15$ (corresponding to the location of peak turbulence intensity contribution). Equation (5) is plotted in figure 6 for $l^+ \approx 34.3$ (grey line) and shows a good agreement when compared to the actual missing two-dimensional energy spectra for $l^+ \approx 34.3$ (black line). Equation (5) can be applied to correct experimental data carried out at similar Re_τ and the wall-normal distance using any hot-wire length in the range $3.8 < l^+ < 57.3$. For correction to one-dimensional energy spectra measured with a single-normal hot wire of a given wire length (l^+), one can integrate equation (5) across the spanwise viscous wavenumber to obtain the following equation for the expected missing energy:

$$\Phi_{uu}^+ \text{ missing}(\lambda_x^+, l^+) = \int f(\lambda_x^+, \lambda_y^+, l^+) d \log(\lambda_y^+). \quad (6)$$

This missing energy can then be added to the measured 1D streamwise energy spectra from the experimental results to obtain an estimate of the true energy spectra at $z^+ \approx 15$.

Figure 7 verifies the validity of the lost spectral energy prediction model using the DNS data. The dashed line shows the unfiltered premultiplied energy spectra calculated from the DNS database at $z^+ \approx 15$. The (---) line shows the spectra calculated with a simulated wire length of $l^+ \approx 34.3$. Clearly there is substantial missing energy for the longer wire as compared to the unfiltered data, particularly at the

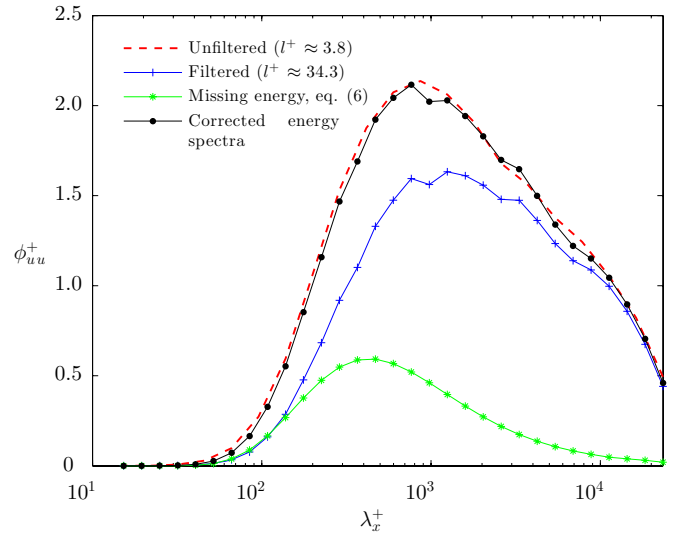


Figure 7. Comparison of the streamwise DNS-corrected energy (—●—) composed of missing energy (—★—), based on equation (6), and filtered energy (---+) using wire length $l^+ \approx 34.4$, against the unfiltered data (solid line, —) at the wall-normal distance $z^+ \approx 15$.

smaller scales. The (---) line shows equation (6) evaluated for $l^+ \approx 34.3$, indicating the predicted missing energy for the given wire length. If the prediction is valid, this line, when added to the filtered spectra, should return an energy distribution close to the original unfiltered data. The (—●—) line is the sum of these two profiles, showing good agreement with the unfiltered DNS energy spectra.

For the model to be practical, it also requires a comparison with data at a different (and higher) Reynolds number than that of the DNS. This is done here by applying the model to the boundary layer data of Hutchins *et al* [10]. The Reynolds number for the boundary layer flow is $Re_\tau \approx 7300$ which is eight times greater than that of the DNS ($Re_\tau \approx 934$). Monty *et al* [19, 20] have shown obvious differences between the large-scale structures in internal and external geometries. However, if we assume that it is mostly small-scale energy that is affected by spatial attenuation (which figure 5 indicates), and that these small scales are universal across channels and boundary layers, we are able to tentatively extend the application of equation (6) to turbulent boundary layers at higher Reynolds numbers. Figure 8 demonstrates exactly how equations (5) and (6) can be used to correct the measured energy spectra from experiments suffering from spatial resolution effects. Figure 8(a) shows experimental hot-wire measured spectra from Hutchins and Marusic [24] at $z^+ \approx 15$ and $Re_\tau \approx 7300$ for three different wire lengths ($l^+ \approx 11, 22$ and 80 , shown by the solid, dashed and dot-dashed lines, respectively). Clearly, the increase in wire length has caused substantial attenuation of the small-scale energetic fluctuations. Figure 8(b) shows the estimated missing energies for each wire length as calculated from equation (5) for the given l^+ and integrated according to equation (6). When these missing energies are added to the original experimental data of plot (a), it is seen that the resulting three corrected energy spectra (shown in figure 8(c))

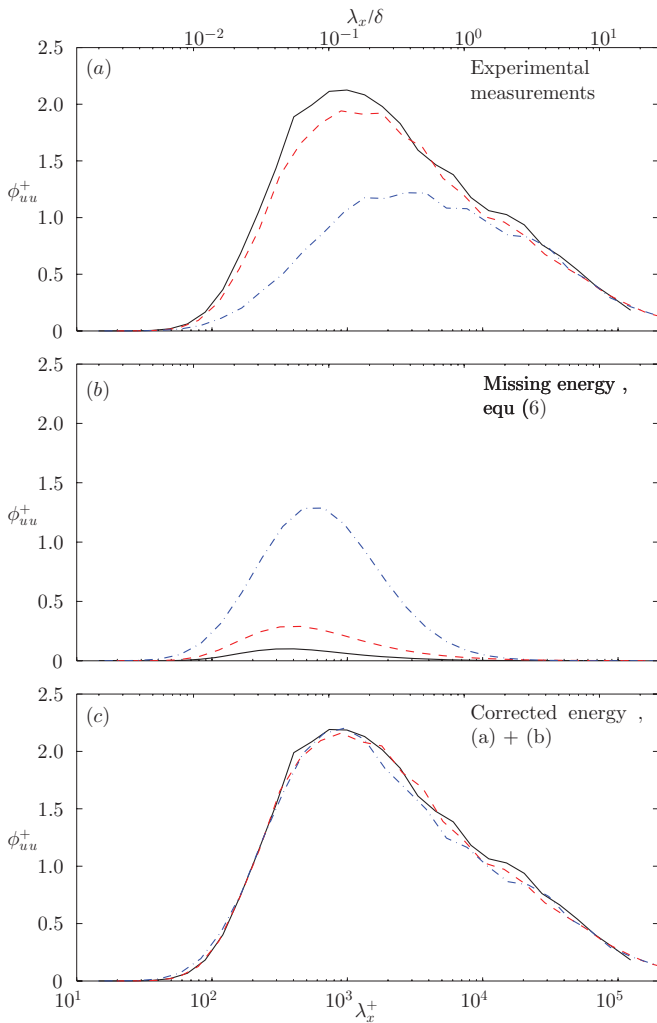


Figure 8. A comparison of the corrected streamwise energy spectra for boundary layer experimental data at $Re_\tau \approx 7300$ for three different wire lengths of $l^+ \approx 11$ (black solid line —), $l^+ \approx 22$ (red dashed line -) and $l^+ \approx 80$ (blue dot-dashed line — · —). (a) shows the actual experimental results, (b) shows the missing energy using equation (6) and (c) shows the corrected energy spectra which is the summation of (a) and (b).

are in very close agreement. All corrected curves have slightly higher peak energy levels than the original $l^+ \approx 11$ experimental data. This is as expected, since equation (5) corrects to an assumed wire length of $l^+ = 3.8$. Provided l/δ is suitably small, application of equation (5) can correct experimental spectra to any simulated wire length l^+ . For example, to correct a measured experimental spectrum (made, say, with a wire of length $l^+ = 22$, as shown by the red dashed curve in figure 8(a)) to the result expected of a different length wire (say $l^+ = 11$), we would simply apply equation (5) to obtain the missing energies for $l^+ = 22$ and for $l^+ = 11$. The difference between these two results, when added to the original measured spectrum, would yield the predicted spectrum for a wire of length $l^+ = 11$.

By calculating the double integrand of the missing energy model (equation 5) with respect to the spanwise and streamwise length scale (λ_y^+ and λ_x^+), one can estimate

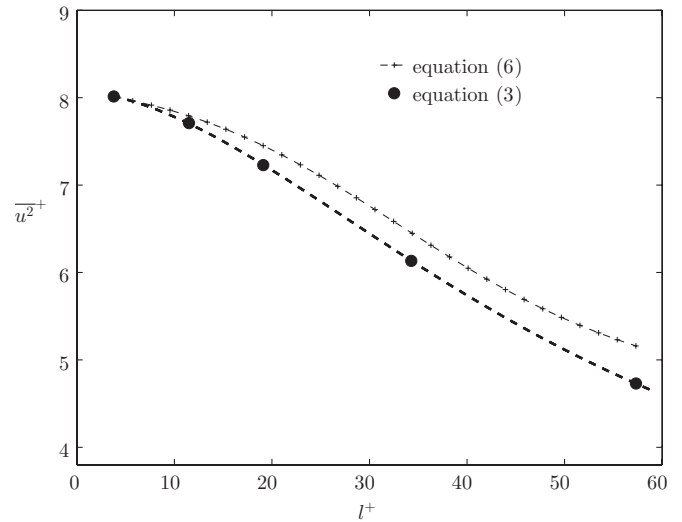


Figure 9. An estimate of the DNS turbulent kinetic energy based on the integral of the lost energy approximation of equation (5) (—+—). The predicted $\overline{u^2}^+$ (—●—) is plotted using equation (3).

the missing broadband energy ($\overline{u^2}^+$) as a percentage of the true turbulent kinetic energy. This result is plotted against equation (3) in figure 9. The results vary slightly, but in general, the missing energy model (based on the 2D premultiplied energy spectra) seems to correctly describe the attenuation in the broadband intensity, with a maximum error of less than 10% occurring at $l^+ \approx 57.3$.

7. Premultiplied two-dimensional energy spectra at $z^+ \approx 120$

In figure 10, the filtered and missing premultiplied two-dimensional energy spectra of the fluctuating u component is shown for different filter lengths at wall-normal location $z^+ \approx 120$. The columns and contour maps are as in figure 5. The peak of the filtered premultiplied two-dimensional energy spectra (column a) seems to remain in approximately the same location as the filter length is increased, contrary to observations closer to the wall in figure 5. At $z^+ = 120$, the most energetic fluctuations have longer characteristic length scales and the contribution due to small-scale structures is negligible; thus, the effect of wire length is less pronounced.

The missing two-dimensional energy spectra are shown in figure 10(b), with the magnitude of the missing energy seen to be notably less than that occurring for $z^+ = 15$ in figure 5 (consistent with the differences in turbulence intensity shown in figure 2). Generally, the results from the missing energy plots of figure 10 indicate that attenuation due to spatial resolution has less effect on the two-dimensional energy spectra as we move further away from the wall (provided that l/δ is not too large). It is also clear that a modified skewed Gaussian model (similar to equation (5)) could potentially also describe the missing two-dimensional energy at $z^+ = 120$.

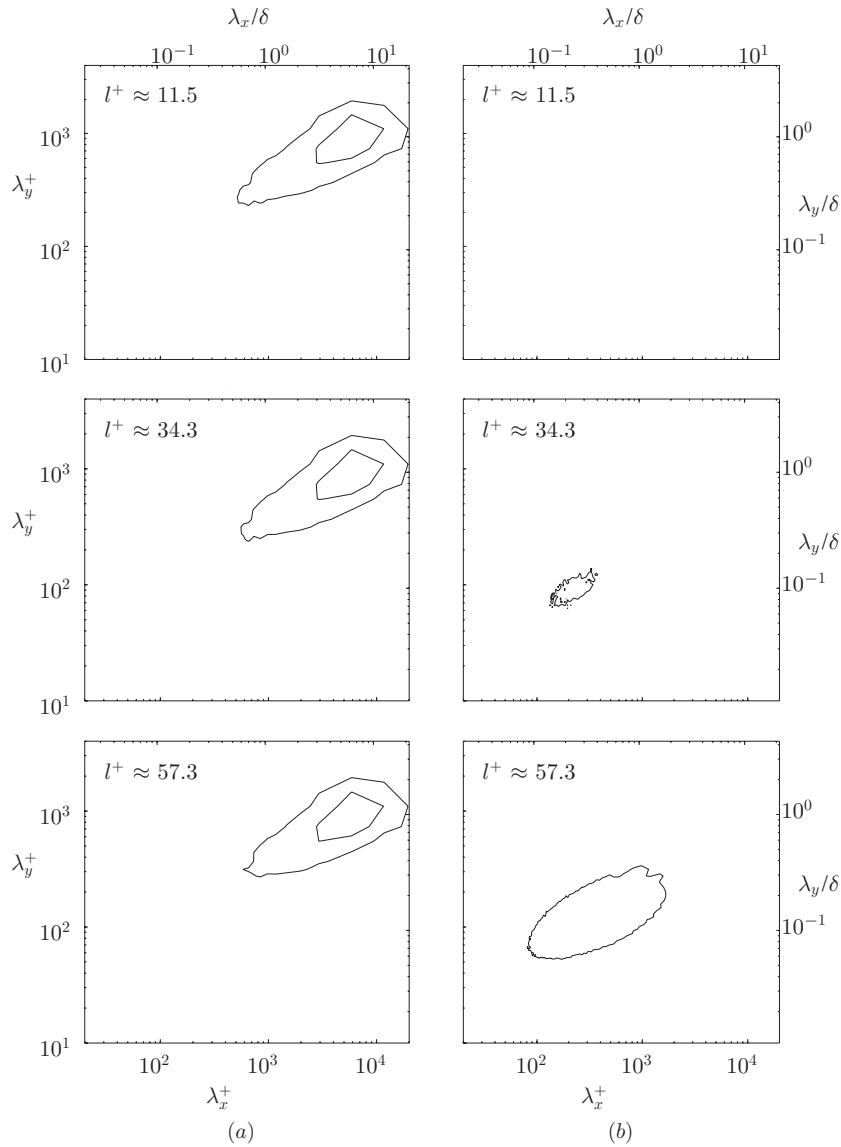


Figure 10. Premultiplied two-dimensional energy spectra of streamwise fluctuating velocity, Φ_{uu}^+ : (a) filtered energy spectra and (b) missing energy spectra, for different filter length (l^+) at wall-normal location $z^+ \approx 120$. Contour levels are as figure 5.

8. Conclusions

The effects of insufficient spatial resolution are investigated through filtering of DNS channel flow data. The turbulence intensity of the filtered streamwise fluctuating component from the DNS is compared with experimental data [7] at a similar Reynolds number (measured with different wire lengths), and similar trends are observed (with increasing attenuation of the turbulence intensity as wire length l^+ increases). The premultiplied two-dimensional energy spectra are examined for different filter lengths at wall-normal locations $z^+ \approx 15$ and 120 . At $z^+ = 15$, it is noted that the attenuation is largely confined to the small-scale near-wall structures, and any superimposed large-scale energy is largely unaffected up to filter lengths of $l^+ \approx 57$. It is also noted that the missing two-dimensional energy can be well-described by a relatively simple modified 2D Gaussian bump (in $\log \lambda_x$ and λ_y). Assuming universality of the near-wall structure,

this missing energy can be assumed to be representative of the attenuation owing to a given viscous-scaled wire length at any Reynolds number. Based on these observations, a missing energy model is proposed. This model is shown to be effective at correcting high Reynolds number ($Re_\tau \approx 7300$) experimental one-dimensional energy spectra at $z^+ = 15$. It is noted that this approach is only valid for situations where the ‘outer site’ (the large-scale energy) has been unaffected by spatial resolution. Thus, this approach will not work for large values of l/δ . The model has been formulated using DNS data up to $l^+ \approx 57$. Beyond these values, the accuracy of the model will likely degrade (although experimental data have proven the accuracy of the model up to $l^+ \approx 80$). Theoretically, within these limits, this model can be used to correct experimental energy spectra for the effects of attenuation due to spatial resolution at any Reynolds number. At present, such a model is only formulated at a single wall-normal position ($z^+ = 15$). However, results at $z^+ = 120$ indicate that this approach can

be expanded to provide a correction to energy spectra at any distance from the wall. In theory, DNS data can provide the information required to extend this model to any value of z^+ . However, such an undertaking (which involves computing 2D energy spectra for several filter lengths at each wall-normal location) was considered beyond the scope of the present work.

Acknowledgments

The authors wish to gratefully thank Professor R D Moser for making the DNS data available, and also the Australian Partnership for Advanced Computing (APAC) and the Victorian Partnership for Advanced Computing (VPAC) for the computational time. The authors gratefully acknowledge the financial support of the Australian Research Council (DP0663499, FF0668703, DP0984577), and the Asian Office of Aerospace Research and Development (AOARD-094023)².

References

- [1] Durst F, Melling A and Whitelaw J H 1976 *Principles and Practice of Laser Doppler Anemometry* (New York: Academic)
- [2] Adrian R J 1991 Particle imaging techniques for experimental fluid mechanics *Annu. Rev. Fluid Mech.* **23** 261–304
- [3] Dryden H L, Shubauer G B, Moch W C and Skramstad H K 1937 Measurements of intensity and scale of wind tunnel turbulence and their relation of the critical Reynolds number of spheres *NACA Technical Report* **581** 109–40
- [4] Frenkiel F N 1949 The influence of the length of a hot wire on the measurements of turbulence *Phys. Rev.* **75** 1263–4
- [5] Wyngaard J C 1968 Measurement of small-scale turbulence structure with hot wires *J. Phys. E: Sci. Instrum.* **1** 1105–8
- [6] Johansson A V and Alfredsson P H 1983 Effects of imperfect spatial resolution on measurements of wall-bounded turbulent shear flows *J. Fluid Mech.* **137** 409–21
- [7] Ligrani P M and Bradshaw P 1987 Spatial resolution and measurement of turbulence in the viscous sublayer using subminiature hot-wire probes *Exp. Fluids* **5** 407–17
- [8] Citriniti J H and George W K 1997 The reduction of spatial aliasing by long hot-wire anemometer probes *Exp. Fluids* **23** 217–24
- [9] Chew Y T, Khoo B C and Li G L 1998 An investigation of wall effects on hot-wire measurements using a bent sublayer probe *Meas. Sci. Technol.* **9** 67–85
- [10] Hutchins N, Nickels T B, Marusic I and Chong M S 2009 Hot-wire spatial resolution issues in wall-bounded turbulence *J. Fluid Mech.* **635** 103–36
- [11] Ewing D and George W K 2000 The effect of cross-flow velocity on mean-square derivatives measured using hot-wires *Exp. Fluids* **29** 418–28
- [12] Abe H, Kawamura H and Choi H 2004 Very large-scale structures and their effects on the wall shear-stress fluctuations in a turbulent channel flow up to $Re_\tau = 640$ *J. Fluid Eng.* **126** 835–43
- [13] del Álamo J C, Jiménez J, Zandonade P and Moser R D 2004 Scaling of the energy spectra of turbulent channels *J. Fluid Mech.* **500** 135–44
- [14] Suzuki Y and Kasagi N 1992 Evaluation of hot-wire measurements in wall shear turbulence using a direct numerical simulation database *Exp. Therm. Fluid Sci.* **5** 69–77
- [15] Moin P and Spalart P R 1987 Contributions of numerical simulation databases to the physics, modelling, and measurement of turbulence *NASA TM 100022*
- [16] Burantini P, Lavoie P and Antonia R A 2008 Velocity derivative skewness in isotropic turbulence and its measurement with hot wires *Exp. Fluids* **45** 523–35
- [17] Vukoslavčević P V, Beratlis N, Balaras E, Wallace J M and Sun O 2009 On the spatial resolution of velocity and velocity gradient based turbulence statistic measured with multi-sensor hot-wire probes *Exp. Fluids* **46** 109–19
- [18] Moin P and Mahesh K 1998 Direct numerical simulation: a tool in turbulence research *Annu. Rev. Fluid Mech.* **30** 539–78
- [19] Monty J P, Stewart J A, Williams R C and Chong M S 2007 Large-scale features in turbulent pipe and channel flows *J. Fluid Mech.* **589** 147–56
- [20] Monty J P, Hutchins N, Ng H C H, Marusic I and Chong M S 2009 A comparison of turbulent pipe, channel and boundary layer flow *J. Fluid Mech.* **632** 431–42
- [21] Kline S J, Reynolds W C, Schraub F A and Runstadler P W 1967 The structure of turbulent boundary layer *J. Fluid Mech.* **30** 741–73
- [22] Jiménez J and Pinelli A 1999 The autonomous cycle of near-wall turbulence *J. Fluid Mech.* **389** 335–59
- [23] Freymuth P 1979 Engineering estimate of heat conduction loss in constant temperature thermal sensors *TSI Quart.* **3** 3–9
- [24] Hutchins N and Marusic I 2007 Evidence of very long meandering features in the logarithmic region of turbulent boundary layers *J. Fluid Mech.* **579** 1–28

² The views and conclusions contained herein are those of the authors and should not be interpreted as necessarily representing the official policies or endorsements, either expressed or implied, of the Air Force Research Laboratory or the US Government.